# Analysing the dynamics of target and spiral waves by image processing techniques

F. G. Jensen*, J. Sporring‡, M. Nielsen§, and P. G. Sørensen*

July 10, 1998

**Abstract**

An algorithm for analysing the evolution of patterns of spirals and target waves in large aspect ratio chemical systems is introduced. The evolutes of target and spiral patterns are used to define their centers, and by the use of Linear Scale-Space a robust method is developed that permits identification of targets and spirals independently of the wave profile. Examples of analysis of long image sequences from experiments with the Belousov-Zhabotinsky reaction catalyzed by ruthenium-tris-bipyridyl are presented. Moving target centers are found. The speed and direction of movement of single as well as double spiral centers are investigated. For the experiments analysed in this paper it is found that the mean velocities of the centers are only locally correlated to the surrounding pattern or to the pattern history.

## 1 Introduction

Target and spiral waves in biological, chemical and physical systems have attracted much attention since the original discovery of such structures in the Belousov-Zhabotinsky (BZ) reaction. Such spatial structures are also observed in convective Rayleigh-Bénard systems, in the aggregating phase of the slime mold *Dictyostelium discoideum* and intercellular $Ca^{2+}$ waves [2, 3, 10, 6]. In real experiments the observed patterns usually appear in the form of multiple target and spiral waves separated by more or less sharp boundaries or by regions of spatio-temporal chaos. In order to analyse the long time dynamics of such systems a huge amount of experimental data must be processed. This type of time consuming analysis is typically performed after the experiments have been conducted, and it has until now only been performed automatically with methods which depend on the special physics or chemistry of the experiment under investigation [4, 12].

The method presented in this paper can identify elliptical and spiral waves independently of the mechanism of the pattern forming system. The method is therefore suitable for analysis of a large class of real as well as computer generated patterns. The method combines filtering techniques known as scale-space methods, differential operators on the image level and statistical methods (see [11] and references therein). The method has time complexity $\mathcal{O}(in \log n)$, where $n$ is the number of pixels and $i$ is the number of images, and it identifies the coordinates of all centers and spiral tips in an image of $256 \times 256$ pixels within 40 sec when implemented in Matlab 5.1 on a HP9000s889 running HPUX 10.20.

In Section 2 the details of the image processing method are described, and in Section 3 spiral and target centers are traced in 12 BZ experiments catalyzed by the metal complex ruthenium-tris-bipyridyl.

*Dept. of Chemistry, University of Copenhagen, Universitetsparken 5, DK-2100 Copenhagen.
‡Dept. of Computer Science, University of Copenhagen, Universitetsparken 1, DK-2100 Copenhagen.
§3DLab, Dept. of Paediatric Dentistry, University of Copenhagen, Nørre Allé 20, DK-2200 Copenhagen.

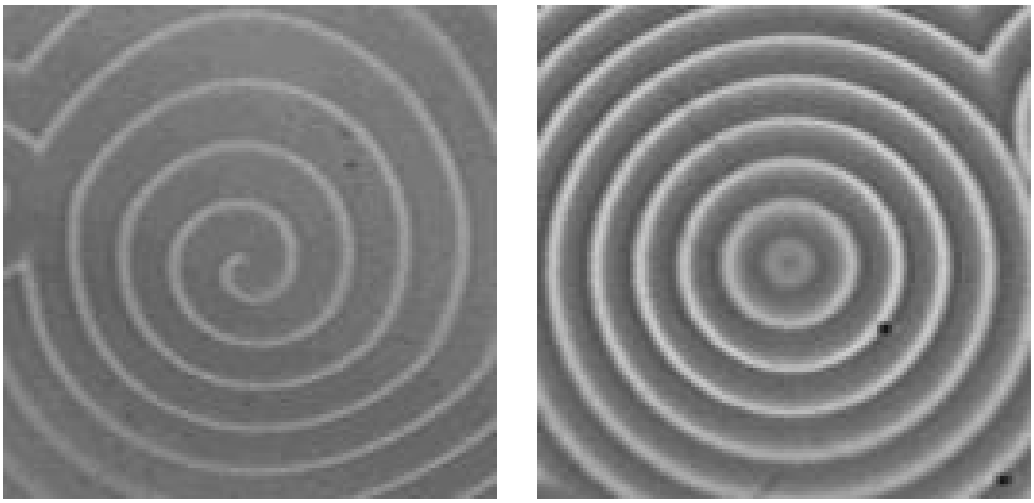

(a) (b)

Figure 1: An example of a spiral (a) and a target pattern (b) in a Belousov-Zhabotinsky experiment with the initial concentrations $[H_2SO_4]$= 0.8 mM, $[BrO_3^-]_0$ = 93.2 mM, $[MA]_0$ = 93.2 mM and $[Ru(bpy)_3^{2+}]_0$ = 0.34 mM.

# 2 An Image Processing Approach

In the following we will describe an image processing approach to the analysis of the dynamics of patterns as generated by the Belousov-Zhabotinsky reaction.

The image model is an intensity surface sampled on a regular spatial grid $(x, y)$, resulting in a matrix of intensity values $L(x, y)$. In Figure 1 are shown images of a target and a spiral pattern from the Belousov-Zhabotinsky reaction.

To study large scale behaviour of spiral patterns Grill *et al.* [4] have used the dynamics of the points of constant intensity (loosely speaking the spiral tip). We have used an alternative approach by noting that the evolute of the wave fronts are compactly located close to the center of the spiral and target pattern. We thus propose to define the center of spiral and target patterns to be the center of the evolute of wave fronts. We will use the dynamics of this center to define the dynamics of the spiral and target patterns. An advantage is that a tracking only depends on the speed of the center and *not* on the rotation rate of the spirals.

## 2.1 Calculating the Evolute

We conceive an image $L(x, y)$ to be a two dimensional manifold in a three dimensional space of two spatial and an intensity coordinate. We will in the following examine the evolutes of isophotes and edges, where isophotes are curves of constant intensity, and edges are the locus of points of maximal intensity change. By examining the intensity change in the gradient direction we find the edges as the following non-linear differential equation:

$$L_{ww} \equiv \frac{L_x^2 L_{xx} + L_y^2 L_{yy} + 2L_x L_y L_{xy}}{L_x^2 + L_y^2} = 0. \tag{2.1}$$

The notation introduced in the above formula is a convenient short-hand and will be used in the rest of this article: $(x, y)$ is the Cartesian spatial coordinates, while $(w, v)$ is a local right hand coordinate system, where $w$ is along the image gradient. This is called the gauge coordinate system. Hence, $L_{ww}$ is the second derivative of $L$ along the $w$ gradient axis. Note that the $(w, v)$

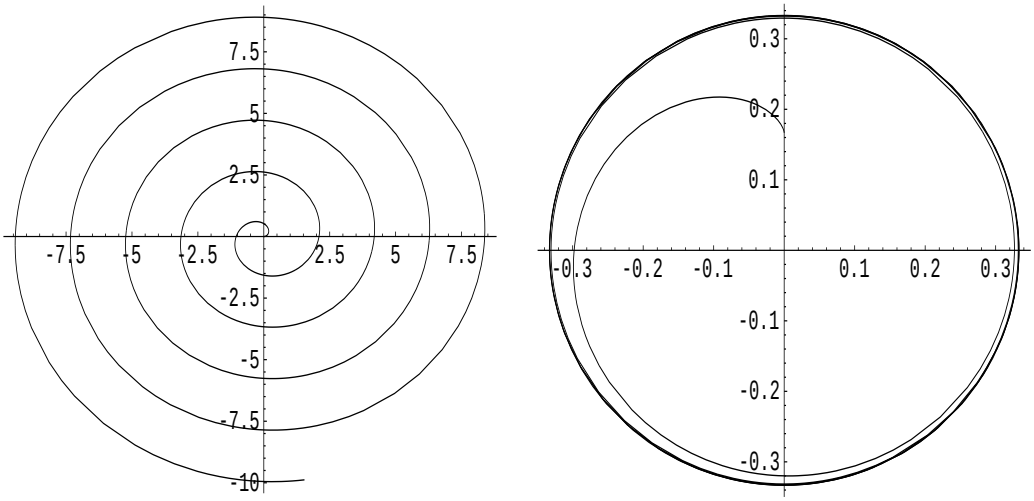


(a) (b)

Figure 2: The spiral: $f(s) = [s\cos(s), s\sin(s)]^T$ (a) and its evolute (b). Note that the evolute is limited by a circle.

coordinate system is undefined in extremal points, where the gradient length $L_w = \sqrt{L_x^2 + L_y^2}$ is zero.

The evolute of a two dimensional curve is defined as the locus of points generated by the center of the osculating circle. For a circle the evolute is a point, and for a symmetrical spiral shown in Figure 2 (a) the evolute is limited by a circle as shown in Figure 2 (b).

The osculating circle is a geometrical interpretation of the curvature $\kappa$ of a two dimensional curve: $1/\kappa$ defines the radius of the circle, and the center lies on the line defined by the curve normal $\vec{N}$.

For an isophote of an image $L$, the normal is along the gradient direction

$$\vec{N} = [L_x, L_y]/\sqrt{L_x^2 + L_y^2}, \tag{2.2}$$

and the curvature is calculated as

$$\kappa \equiv \frac{L_{vv}}{L_w} \equiv \frac{L_x^2 L_{yy} + L_y^2 L_{xx} - 2L_x L_y L_{xy}}{(L_x^2 + L_y^2)^{3/2}}, \tag{2.3}$$

Due to the discrete nature of images, edges will also be a discrete set of points and therefore also the evolute. Hence we work with the following set:

$$\alpha_k = \{[x, y] + \kappa^{-1}\vec{N} | L(x, y) = k\}, \tag{2.4}$$

and the set of points $L(x, y) = k$ will be extended by bilinear interpolation in $L$.

The evolute of the $L_{ww} = 0$ edges is estimated in the same manner as above simply by replacing $L$ with $L_{ww}$ in all the above equations and setting $k = 0$, i.e. evaluating on the zero isophote of $L_{ww}$. For example, the curvature is found by

$$\kappa' \equiv \frac{L_{wwx}^2 L_{wwyy} + L_{wwy}^2 L_{wwxx} - 2L_{wwx} L_{wwy} L_{wwxy}}{(L_{wwx}^2 + L_{wwy}^2)^{3/2}}. \tag{2.5}$$

In this case up to fourth order derivatives are used to extract the curvatures on the edges. Note that $\kappa' \neq L_{wwvv}/L_{www}$ since $L_{ww}$ has a different gauge coordinate system than $L$.

The image derivatives can conveniently be estimated using Linear Scale-Space (see [11] and the references therein), i.e. smoothing the image with a Gaussian kernel of standard deviation $\sqrt{2t}$,

$$L(x, y, t) = G(x, y, t) * L(x, y), \tag{2.6}$$

where the original image is $L(x, y)$ and $t$ is the scale. The advantage of such an embedding is that it reduces the grid and noise effects, allows for a uniform analysis of image structures at all scales, and allows for a well posed estimation of spatial derivatives,

$$L_{x^i y^j}(x, y, t) = G_{x^i y^j}(x, y, t) * L(x, y).$$

In this manner, taking image derivatives of fourth or higher orders is not an unprecise process (see [1, 5] for a noise analysis).

We will now demonstrate the difference between the isophotes and the edge approaches on a single image. In Figure 3, a single isophote has been shown for the two images together with the corresponding evolute set using Equation 2.3. Immediately we observe that the isophotes are very dependent on the large scale image behaviour. The spiral is for example lighter at the top than at the bottom, hence the isophotes can be seen as a dividing line. In this case heuristics must be introduced, and all isophotes with the large gradient lengths are included in the estimate. Still, the drawback of the evolutes of the isophotes is that they are only loosely coupled to the wave fronts.

In contrast as shown in Figure 4, we demonstrate the use of the curvature of the edges given by Equation 2.5. As it is seen, the edges follow the stripe structure better and the evolute set is less noisy.

### 2.2 Analysing the Dynamics of the Evolute

Each point on the edge contributes with one point on the evolute. Some of the points will be unrelated to the spiral or the target patterns and may be interpreted as noise in the image, and some will be situated in clusters. For computational reasons, the easiest method of finding the cluster centers is to sample the evolute points on a regular grid, e.g. the same grid as the image is given by, and use Linear Scale-Space to locate the maxima. The scale-space may be applied in two ways: Either by finding extremal points image by image or by stacking the images into a single three dimensional image and locating the three dimensional ridge of extremal points. The latter very reasonably implies that the dynamics is continuous, and it is even possible to implement time causal algorithms that only use past data. But to achieve maximal speed we have chosen to implement the image by image analysis.

To validate the definition of the spiral center, a stable spiral generated by a numerical simulation has been investigated as shown in Figure 5. The simulated model is a three variable autocatalator [7]. The simulation is performed on $256 \times 256$ grid using a simple 5 point discrete Laplace operator. The spiral tip performs a cycloid motion as shown in Figure 5 (c). In this case the program detects the center of the spiral but without the cycloid motion as seen in (b).

## 3 The Experiments

The chemicals used in the experiments were prepared from potassiumbromat (Riedel-de Haën 30205), malonic acid (Aldrich M129-6), $Ru(bpy)_3Cl_2$ (Fluka 93307 Tris(2,2'-bipyridyl)ruthenium(II)-chloride Hexahydrate), sulfuric acid (J.T. Baker) and double distilled water. The chloride ions of the catalyst complex were replaced with sulfate ions using a column. The product was tested with a chloride selective electrode.

The experiments were performed in a 9 cm Petri dish and the reaction layer was 0.85 mm tick i.e. the aspect ratio $\Gamma_{\text{ext}} > 100$. The dish was placed in a thermostated compartment held at $25 \pm 0.1\,^{\circ}\text{C}$, which was loaded with $N_2$ gas to avoid surface reactions between the reactants

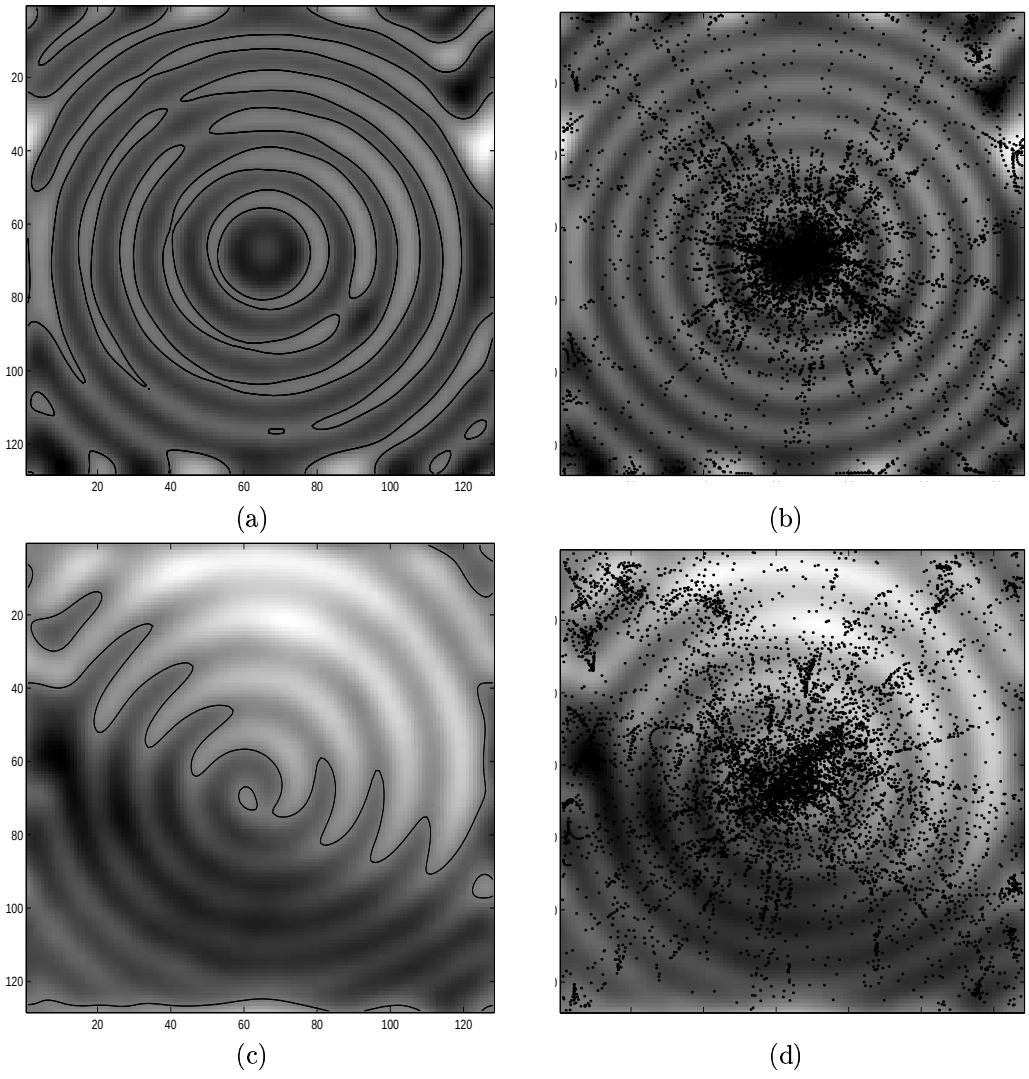


Figure 3: The above images show a single isophotes (black lines) for the target pattern (a) and the spiral (c), and the corresponding evolute sets (b) and (d) taken where the gradient is high and at scale $t = 8$.

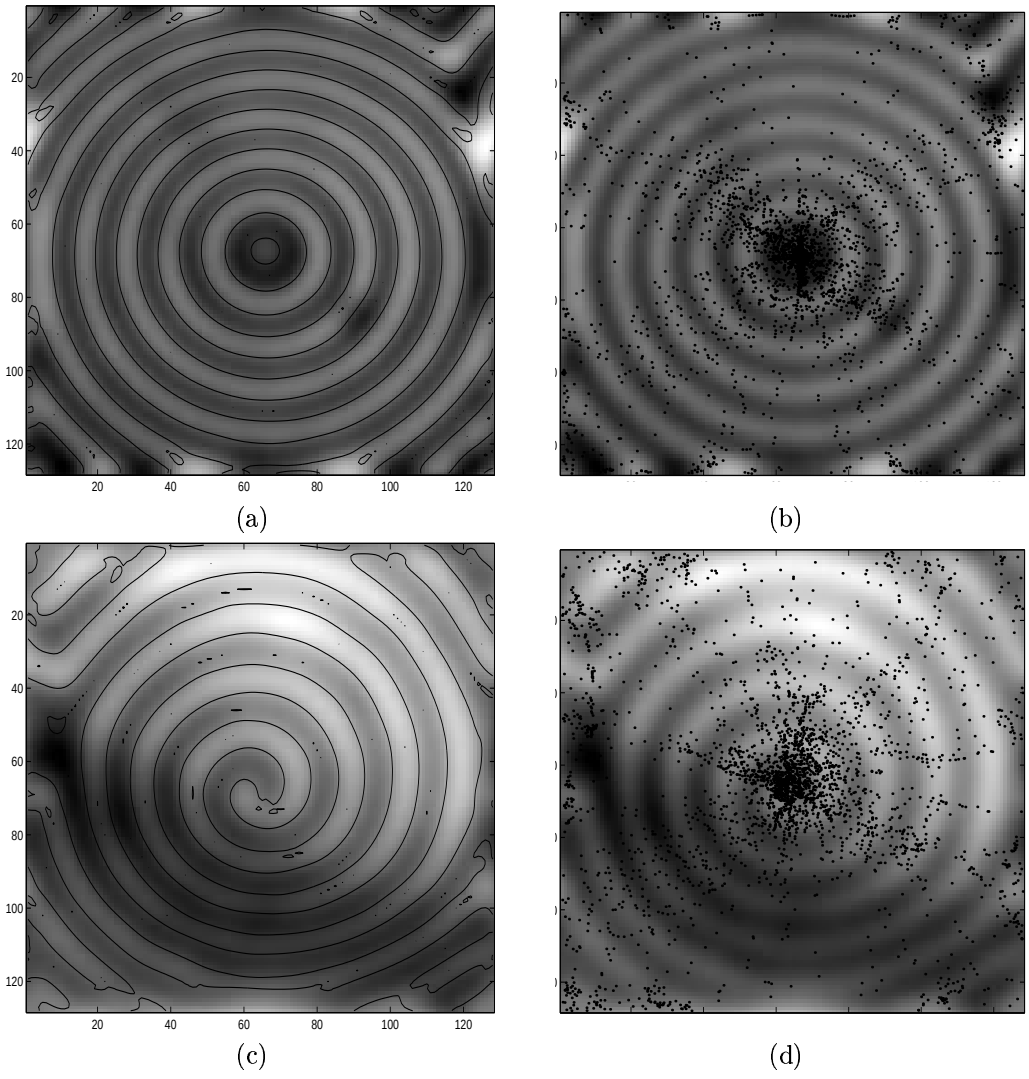


Figure 4: The above images show the edge lines ($L_{ww} = 0$) for the target pattern (a) and the spiral (c) and the corresponding evolute sets (b) and (d) taken where the gradient is high and at scale $t = 8$.

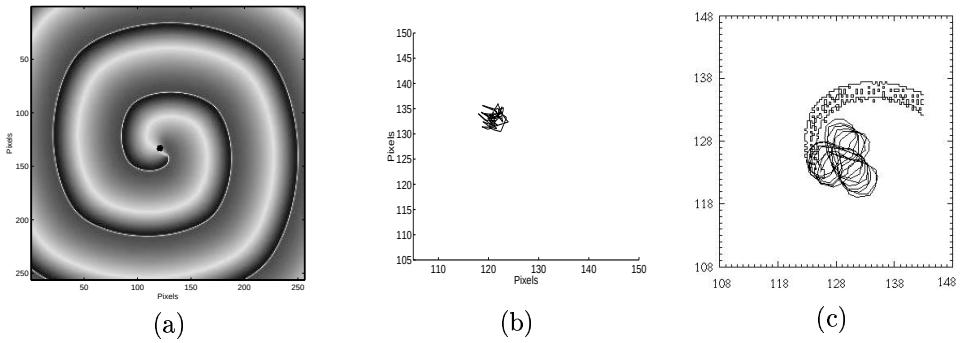


(a) (b) (c)

Figure 5: Validating the method on a simulated system. (a) shows the image of one component of a simulation of a spiral. The tip is moving. In (b) the detection of the center is shown. No cycloid motion is detected. In (c) a magnification of the motion of the spiral tip is shown. Here cycloid movement is seen.

and oxygen in the atmosphere above the solution. The layer was illuminated from below with a 300 W Xenon arc lamp (Oriel model 66083). The lamp was equipped with a UV grade fused condenser and a photo-feedback system (Oriel model 68850) to obtain a homogeneous distribution of the light on the reaction layer. The light of illumination passed through a central bandwidth filter of 450 $\pm$ 10 nm. (Spindler & Hoyer). The intensity of the light in the reaction layer was $120 \pm 10$ nWcm$^{-2}$. Such low intensity does not perturb the chemistry of the chemical reactions, and in the following we do not consider any interactions between catalyst and light. Nevertheless, we obtained images with high contrast between the oxidised and the reduced areas of the reaction solution. The images of the reaction were captured with a CCD camera (VarioCam PCO CCD) with $720 \times 540$ imaging pixels, zoom optics (Fujinon TV-Z 1:18/12.5-75) and a frame-grabber (Imagraph Imascan Chroma-P) before they were stored on a PC. After mixing the chemicals the reaction solution was covered and left undisturbed. Band of travelling waves, oscillating centers and spirals developed spontaneously in the reaction layer, and we followed the evolution of the patterns until they disappeared, in some cases for more than 1 hour depending on the concentrations of the chemicals.

The program is able to identify target centers. Waves emitted from such centers are often only visible for short time compared to spiral centers, since target centers are annihilated by travelling waves in the reaction layer because of their lower frequency. An other complication is that long living target centers in ruthenium catalyzed experiments eventually become distorted from circular to elliptic geometry, or even more irregular shapes. Target centers in the ruthenium catalyzed reaction can move through the reaction solution, as it is seen in Figure 6. This center is detected by the program through 14 min, in which it moves 5.6 mm with a mean speed of 0.39 mmmin$^{-1}$. The speed of the center is not constant within the time interval it was observed. The speed oscillates aperiodic around a mean value, such that the position of the target center is some times almost fixed, while occasionally it moves through the solution.

In total we have traced the paths of 37 spiral centers in 12 experiments with different $[H_2SO_4]$, $[BrO_3^-]_0$ and $[MA]_0$, which are the main reactant concentrations. The initial concentration of the catalyst is fixed to 0.34 mM in all experiments. In Table 1 the characteristics of 12 paths are listed, together with the different combinations of the chemicals used. The subscript numbers refer to a numbering of the trajectories observed in the same experiment. Note, in this table how centers detected in the same experiment can have different mean speeds.

Figure 7 shows trajectories of motion of spiral and target centers in six different experiments. The trajectories are superimposed on images taken halfway through each experiment. The analysis is performed for all the subimages indicated by black squares. The examples were selected to show typical types of motion of the observed patterns. The experiments ru101

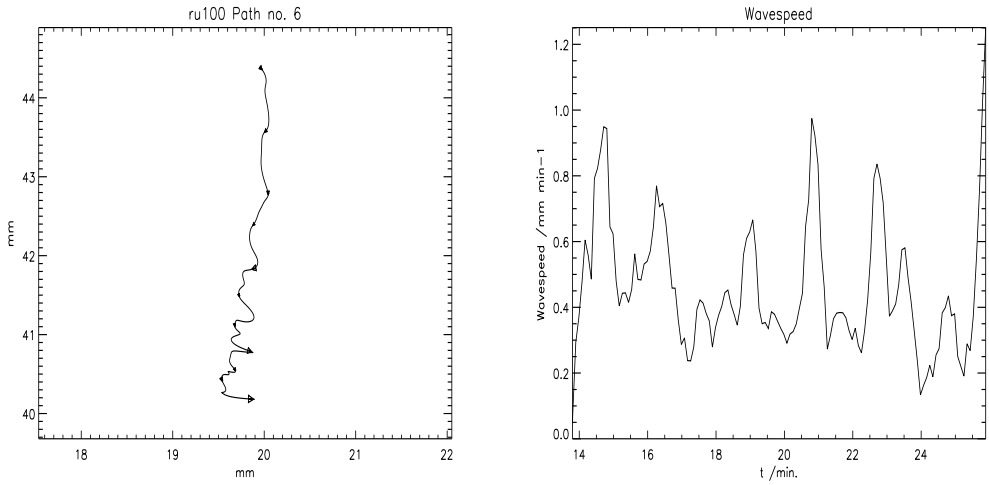


(a) (b)

Figure 6: In (a) the path of a target center is shown for an experiment with $[H_2SO_4]$= 0.4 M, $[BrO_3^-]_0$ = 93.2 mM and $[MA]_0$ = 93.2 mM. The arrows indicate the direction of movement. In (b) the mean velocity of the target center is shown as function of time.

| Name: | $[H_2SO_4]$ /M | $[BrO_3^-]_0$ /mM | $[MA]_0$ /mM | Length /mm | Time /sec. | $< v >$ /mm sec$^{-1}$ |
|---|---|---|---|---|---|---|
| $ru233_1$ | 1.0 | 93.2 | 93.2 | 6.8 | 59.0 | 0.11 |
| $ru238_4$ | 1.0 | 46.6 | 93.2 | 16.6 | 44.0 | 0.36 |
| $ru237_1$ | 1.0 | 46.6 | 139.8 | 7.2 | 16.0 | 0.44 |
| $ru202_1$ | 0.8 | 139.8 | 139.8 | 8.4 | 29.0 | 0.28 |
| $ru208_3$ | 0.8 | 93.2 | 93.2 | 5.6 | 42.0 | 0.13 |
| $ru213_4$ | 0.8 | 93.2 | 46.6 | 12.9 | 36.0 | 0.35 |
| $ru213_3$ | 0.8 | 93.2 | 46.6 | 20.6 | 46.0 | 0.45 |
| $ru100_3$ | 0.4 | 93.2 | 93.2 | 11.0 | 54.0 | 0.20 |
| $ru100_4$ | 0.4 | 93.2 | 93.2 | 11.4 | 54.0 | 0.21 |
| $ru101_{10}$ | 0.4 | 93.2 | 46.6 | 18.6 | 50.0 | 0.37 |
| $ru101_9$ | 0.4 | 93.2 | 46.6 | 11.5 | 48.0 | 0.23 |
| $ru119_1$ | 0.2 | 233.1 | 93.2 | 7.8 | 23.0 | 0.33 |

Table 1: The characteristics of 12 spiral centers detected in 9 different experiments. The subscripts on the name of the paths refer to different paths detected in the same experiments.

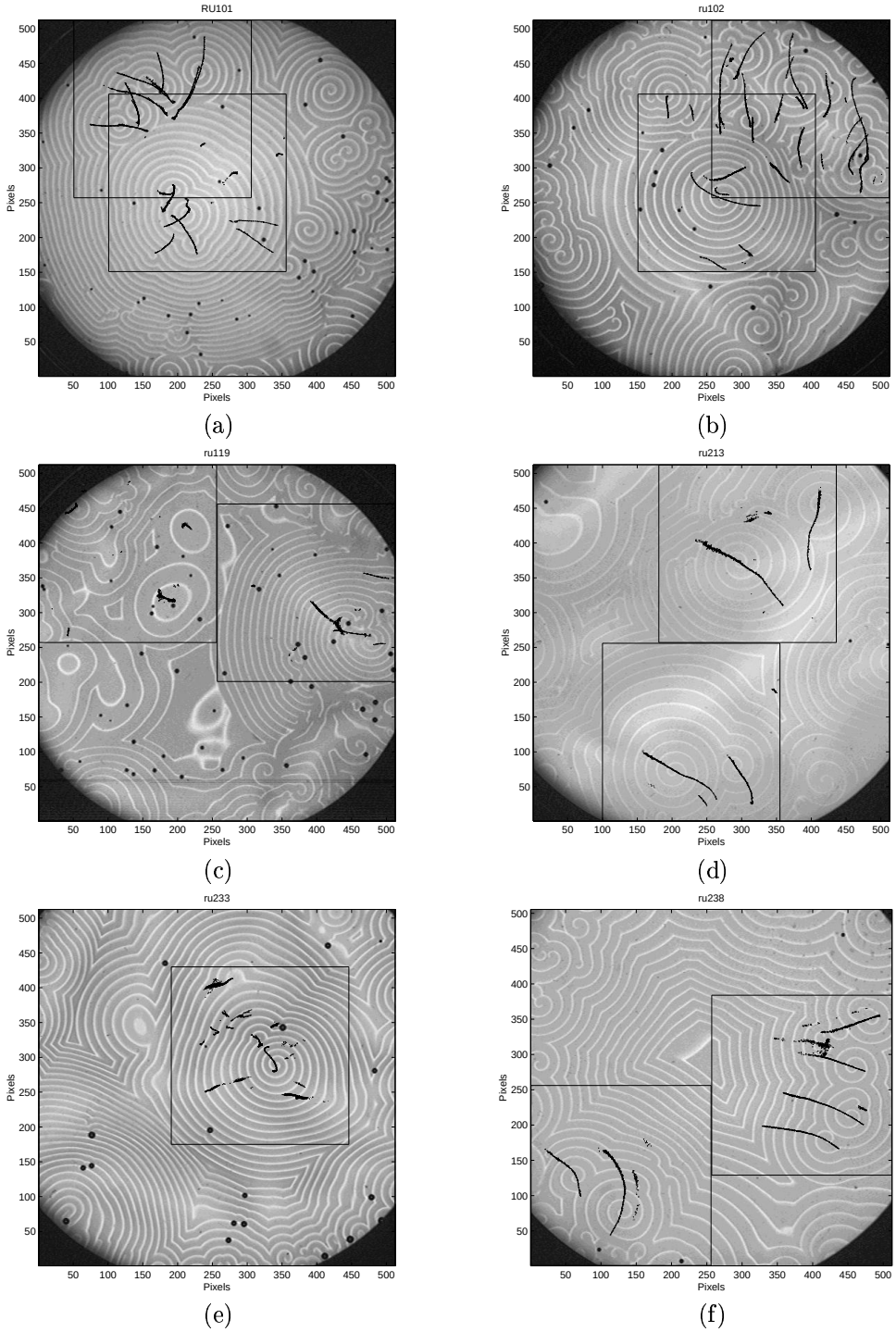


Figure 7: Examples of large scale motion of a spiral and target pattern. The movement of the centers are shown superimposed on the midway image. The $256 \times 256$ subimage analyzed is indicated by a box. Not all of the patterns found are present at the shown time, and in general the target patterns are much more unsymmetrical than the spirals. E.g. in (e) the noisy paths are due to early target patterns.

Figure 7 (a) and ru102 Figure 7 (b) are typical and contain mainly spiral centers moving along straight or slightly bended curves. In experiment ru102 Figure 7 (b) a big spiral in the center of the image moves perpendicular to the trajectories of the other detected centers to the upper left in the image. In experiment ru119 Figure 7 (c) the reaction becomes turbulent a short time after the shown image, and the spiral dissolves in turbulent waves without any detectable centers. Experiment ru213 Figure 7 (d) shows a successful tracking of centers in an image with very low contrast between the oxidised and the reduced parts of the reaction solution. Experiment ru233 Figure 7 (e) demonstrates a complicated *s*-shaped movement of a spiral center. In this experiment the noisy paths are due to some early very elongated target patterns, for which it is difficult to define a true center. The experiment ru238 Figure 7 (f) shows bended as well as almost straight trajectories within the same experiment.

For the spiral centers we find, that the mean speed of different centers observed in the same experiment can vary more than a factor 1.5, see Table 1. In all experiments the spiral centers move, but characteristics such as the length of the paths, the observation time and the mean speed of the centers are different. Under our experimental conditions we have not been able to relate the mean speed of a spiral center to $[H_2SO_4]$, $[BrO_3^-]_0$ or $[MA]_0$. This property of spiral centers is in contrast to the empirical relation found by Ram Reddy *et al.* [8] for the velocity of travelling waves: $v \propto \sqrt{[H_2SO_4][BrO_3^-]}$. As an example we find the fastest moving spiral center has $< v >= 0.45$ mm min$^{-1}$ at $[H_2SO_4]= 0.8$ M, $[BrO_3^-]_0 = 93.2$ mM and $[MA]_0 = 46.6$ mM; while the slowest moving center with $< v >= 0.13$ mm min$^{-1}$ is found at almost identical reactant concentrations $[H_2SO_4]= 0.8$ M, $[BrO_3^-]_0 = 93.2$ mM and $[MA]_0 = 93.2$ mM. See the trajectories $ru213_3$ and $ru208_3$ in Table 1. In both experiments the velocities persisted for more than 45 min. The speed of the moving spiral centers can be grouped in three different types as it is illustrated in Figure 8 for three typical systems. The mean speed of the center shown in Figure 8 (a) is initially decreasing, later it becomes almost constant. This is the most common development observed. In Figure 8 (b) the speed oscillates slightly around its mean value throughout the experiment, and the spiral moves with almost constant velocity. The fluctuations at the end of the detection period are due to noise. The mean speed of the center shown in Figure 8 (c) initially is growing until it passes through a maximum and decreases to the original value again. The trajectory corresponding to this velocity profile is seen in Figure 7 (e).

The directions in which the spiral centers move can also be grouped into three types. These are shown in Figure 9. The most typical shapes of the trajectories are slightly curved paths as shown in Figure 9 (a). This path is 20.6 mm long, and the spiral center is first detected in the interior of the dish. The center is also seen in Figure 7 (d). When several centers are detected in the same area of the reaction layer they will most often move in the same direction, as it is seen in the experiment ru101 in Figure 7 (d) and (f). The trajectory shown in Figure 9 (b) is an example of a more curved path, where the direction of movement turns nearly 360 degrees within the 54 min the center is observed. The characteristics of this center and a nearby detected center are both listed in Table 1. These two centers have almost identical mean speeds. In Figure 9 (c) an example of a *s*-shaped curve is shown. This spiral center is observed in 1 hour, but the speed of the center is slow.

In several cases, spirals are initially formed as pairs of counter rotating centers. Each spiral can then grow, if the distance between the centers grow during time. We have investigated the double spiral centers formed spontaneously in the experiments in order to detect similarities and differences in such pairs. In Table 2 we list the characteristics of 6 centers. The first 4 centers are formed as pairs. The 2 last centers develop closed to each other in the experiment ru213 are listed for comparison. In Figure 10 the typical development of the trajectories of a double center is shown in (a). In (b) the distance between the 2 centers as function of time is shown. Spontaneously formed double centers are common in our experiments, but many centers do not move away from each other. If the spiral centers, however, drift away from each other then the separation distance grows linearly with constant speed as shown in the plot. In Figure 10 (c) an example of two atypical centers are shown. These centers are also initially

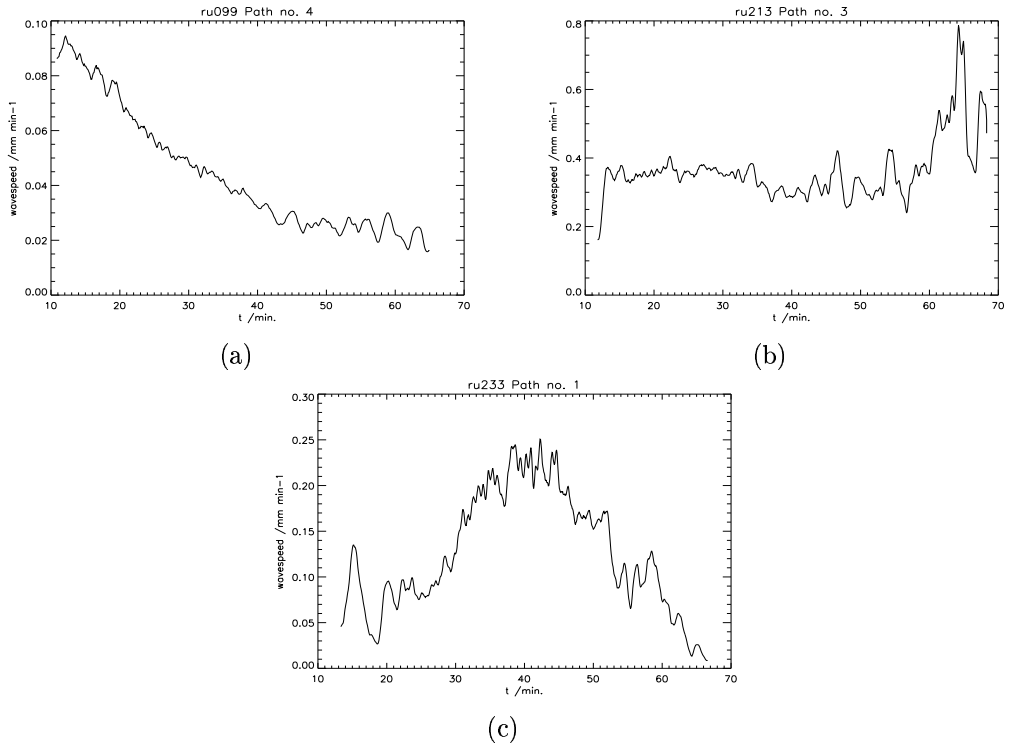


Figure 8: The time development of the speed of three spiral centers detected in the experiments ru099, ru213 and ru233 with the following initial conditions. (a): $[H_2SO_4]$= 0.4 mM, $[BrO_3^-]_0$ = 93.2 mM, $[MA]_0$ = 93.2 mM. (b): $[H_2SO_4]$= 0.8 mM, $[BrO_3^-]_0$ = 93.2 mM, $[MA]_0$ = 46.6 mM. (c): $[H_2SO_4]$= 1.0 mM, $[BrO_3^-]_0$ = 93.2 mM, $[MA]_0$ = 93.2 mM.

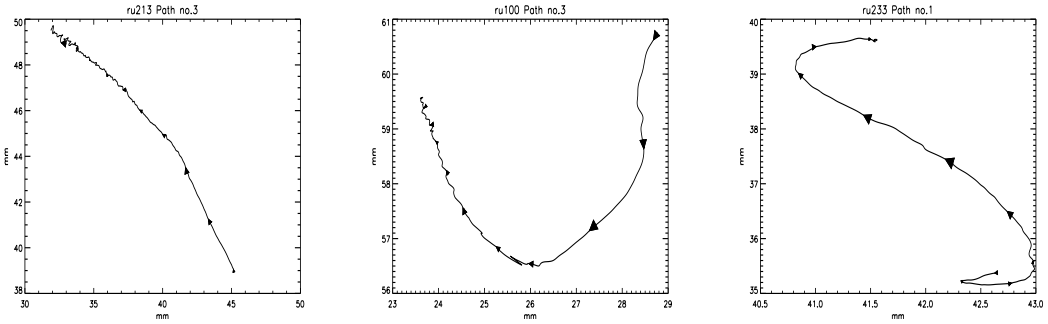


Figure 9: Three typical trajectories of spiral centers. The initial conditions are: (a): $[H_2SO_4]$= 0.8 mM, $[BrO_3^-]_0$ = 93.2 mM, $[MA]_0$ = 46.6 mM; (b): $[H_2SO_4]$= 0.4 mM, $[BrO_3^-]_0$ = 93.2 mM, $[MA]_0$ = 93.2 mM, and to the (c): $[H_2SO_4]$= 1.0 mM, $[BrO_3^-]_0$ = 93.2 mM, $[MA]_0$ = 93.2 mM.

| Name: | $[H_2SO_4]$ /M | $[BrO_3^-]_0$ / mM | $[MA]_0$ mM | Length | Time | $< v >$ |
|---|---|---|---|---|---|---|
| $ru099_3$ | 0.4 | 93.2 | 93.2 | 7.6 | 33.0 | 0.23 |
| $ru099_8$ | 0.4 | 93.2 | 93.2 | 16.6 | 54.0 | 0.31 |
| $ru101_3$ | 0.4 | 93.2 | 46.6 | 9.1 | 34.0 | 0.26 |
| $ru101_4$ | 0.4 | 93.2 | 46.6 | 9.3 | 54.0 | 0.17 |
| $ru213_3$ | 0.8 | 93.2 | 46.6 | 20.6 | 46.0 | 0.45 |
| $ru213_4$ | 0.8 | 93.2 | 46.6 | 12.9 | 36.0 | 0.35 |

Table 2: Characteristics of the paths traced by two double centers in the experiments ru099 and ru101 and two single centers in the same part of the dish in the experiment ru213. The speed is of the individual centers. The indices in the first column refer to different paths in the same experiment.

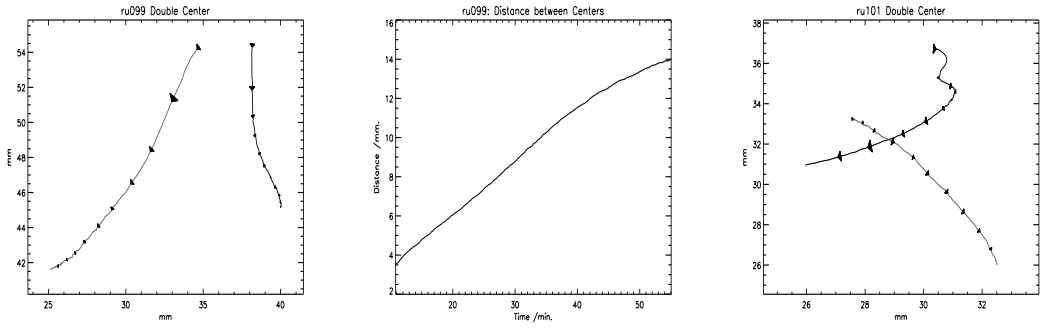


(a) (b) (c)

Figure 10: In (a) is shown the trajectories of two spiral centers initially formed as a double spiral with reactant concentrations $[H_2SO_4]$= 0.8 mM, $[BrO_3^-]_0$ = 93.2 mM, and $[MA]_0$ = 93.2 mM. In (b) the separation distance between the two centers shown in (a) are calculated as function of time. It is seen that the distance between the centers grows almost linearly. In (c) are shown the trajectories of the two centers which also initially are formed as a double center. But in this case the centers move in a fashion so their trajectories cross.

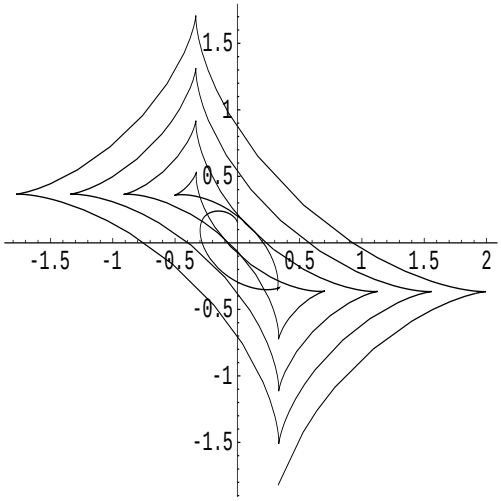


Figure 11: The resulting evolute when the aspect ratio of the coordinate system is 1.1, i.e. $f(s) = [s\cos(s), 1.1s\sin(s)]^T$. This evolute has no limiting area.

formed as a pair.

The diameter of the petri dish is 9 cm. In most cases the we find the direction and velocity of different centers are related over short distances, but unrelated over distances comparable to the diameter of the petri dish. It is not likely that convection in the reaction layer causes the movements of the centers, since the reaction layer is very thin. This is in agreement with observations made by e.g. Rodriguez and Vidal [9]. The zones of coherence which are spontaneously established are separated by zones of annihilation of waves. The coherence zones form a superstructure which persists over long time but change eventually. Such coherence zones can be seen in all experiments shown in Figure 7.

# 4 Discussion

An system for automatic tracing of large scale dynamics of spiral and target waves has been presented. It uses a new operational definition of the center of spiral and target waves based on the evolute of the waves. Although computation of the evolute as presented here uses up to fourth order spatial derivatives, it is very stable both with respect to contrast and noise. This is due to the use of the Linear Scale-Space techniques and natural integration over a large support.

Note, however, the evolute of an ellipse ($f(s,k) = [\cos(s), k\sin(s)]^T, k \neq 1$) and an 'oval' spiral ($f(s,k) = [s\cos(s), sk\sin(s)]^T, k \neq 1$) does not have compact support with a well defined density maximum. See e.g. Figure 11 where an example of the evolute for an oval spiral is shown. This does not seem to be a problem for the real target and spiral waves observed in these experiments, which evolve towards regular patterns with compact support.

In the current implementation the processing time is approximately 40 seconds for a 256x256 image using a Matlab 5.1 implementation running on a HP9000s899 under HPUX 10.20. A preliminary study indicates that it may be possible to reduce the processing time by an order of magnitude.

The presence of spiral or target waves can be distinguished by a simple local analysis around the center as follows: Draw a circle of radius larger than the wave length around the center and count the number of transitions encountered. If an odd number of transitions is found, the density maximum is a center for a spiral, otherwise it is a center for a target wave. In this way the method enables quantitative and automatic identification of spiral and target patterns in

experimental data.

By preliminary experiments we expect that other types of geometrical wave configurations may be identified by the use of Linear Scale-Space, e.g. the cusp in the interface between two planar waves. This is left for further development.

From the application of the method to large aspect ratio wave patterns in the ruthenium catalyzed BZ reaction we have found no simple correlations between the patterns of waves of the individual centers and the concentrations of the main reactants. We have, however, found a strong indication of local correlation of the speed and movement of centers arranged in a slowly changing superstructure of regions, but a detailed explanation requires more experiments.

# References


[1] J. Blom, B. M. ter Haar Romeny, A. Bel, and J. J. Koenderink. Spatial derivatives and the propagation of noise in Gaussian scale-space. *Journal of Visual Communication and Image Representation*, 4(1):1–13, March 1993.

[2] M.C. Cross and P.C. Hohenberg. *Pattern formation outside equilibrium*, volume 65, chapter 1, pages 854–865. The American Physical Society, July 1993.

[3] R.J. Field and M. Burger. *Oscillations and Traveling Waves in Chemical Systems*. J. Wiley & Sons, New York, 1985.

[4] S. Grill, V. S. Zykov, and S. C. Müller. Spiral wave dynamics under pulsatory modulation of excitability. *J. Phys. Chem.*, 100(49):19082–19088, 1996.

[5] B. M. ter Haar Romeny, W. J. Niessen, J. Wilting, and L. M. J. Florack. Differential structure of images: Accuracy of representation. In *Proc. First IEEE Internat. Conf. on Image Processing*, pages 21–25, Austin, TX, November13–16 1994. IEEE.

[6] J.D. Lechleiter and D.E. Clapham. Molecular Mechanisms of Intracellular Calcium Excitability in X. laevis Oocytes. *Cell*, Vol. 69:284–294, April 17 1992.

[7] B. Peng, S. K. Scott, and K. Showalter. Period doubling and chaos in a three-variable autocatalator. *J. Phys. Chem.*, 94(1):5243, 1994.

[8] M.K. Ram Reddy, Zs. Nagy-Ungvarai, and S.C. Müller. Effect of Visible light on Wave Propagation in the Ruthenium-Catalyzed Belousov-Zhabotinsky Reaction. *J. Phys. Chem.*, 98:12225–12259, July 1994.

[9] J. Rodriguez and C. Vidal. Measurement of Convection Velocities in "Mosaic" Patterns. *J. Phys. Chem.*, 93(7):2737–2740, 1989.

[10] F. Siegert and C.J. Weijer. Analysis of optical density wave in propagation and cell movement in the cellular mould *Dictyostelium discoideum*. In H.L. Swinney and V.I. Krinsky, editors, *Waves and Patterns in Chemical and Biological Media*, volume 49 of *Physica D*, pages 224–232. First MIT Press, Elsevier Science Publishers,B.V.Amsterdam,the Netherlands, 1992.

[11] J. Weickert, S. Ishikawa, and A. Imiya. On the history of Gaussian scale-space axiomatics. In Jon Sporring, Mads Nielsen, Luc Florack, and Peter Johansen, editors, *Gaussian Scale-Space Theory*, pages 45–59. Kluwer Academic Publishers, Dordrecht, The Netherlands, 1997.

[12] A.T. Winfree, S. Caudle, G. Chen, P. McGuire, and Z. Szilagyi. Quantitative optical tomography of chemical waves and their organizing centers. *Chaos*, 6(4), 1996.